How to observe the elusive resonances in hydrogen atom or deuterium atom + molecular hydrogen .fwdarw. molecular hydrogen or hydrogen deuteride + hydrogen atom reactive scattering

ARTICLE *in* THE JOURNAL OF PHYSICAL CHEMISTRY · JANUARY 1991

Impact Factor: 2.78 · DOI: 10.1021/j100154a007

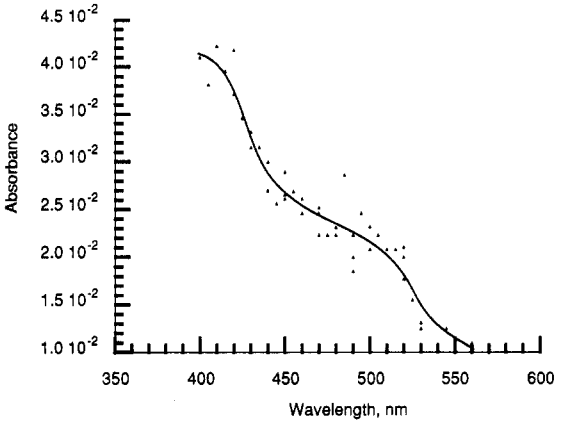

Figure 1. Triplet-triplet absorption spectrum of C_{60} in benzene.

$\pm$ 0.05 (355 nm) and 0.96 $\pm$ 0.04 (532 nm). Formation of $^1O_2$ occurs by energy transfer from the highly populated C_{60} triplet state to molecular oxygen. These values represent a lower limit for the quantum yield of triplet production (Φ_T).

(12) Ogilby, P. R.; Foote, C. S. *J. Am. Chem. Soc.* **1982**, *104*, 2069.

The lower singlet oxygen quantum yield at 355 nm appears to be outside the experimental error and is currently being investigated. One possible explanation is that there is a lower intersystem crossing yield from upper singlet excited states than from S_1. The higher singlet states may be connected with additional deactivation channels which compete with ISC.

C_{60} also quenches singlet oxygen with an approximate rate constant $k_q(^1O_2) = (5 \pm 2) \times 10^5$ M^{-1} s^{-1}, as shown by a small shortening of the lifetime of the singlet oxygen luminescence with a nearly saturated solution of C_{60} in C_6D_6. The mechanism of quenching by C_{60} is presently unknown; chemical reaction is unlikely because no loss of starting material or formation of new product (by UV-visible absorption spectra) occurs following hundreds of laser pulses under O_2 at either excitation wavelength.

C_{60} is a potent generator of singlet oxygen. Its very high singlet oxygen yield and inertness to photooxidative destruction suggests a strong potential for photodynamic damage to biological systems. Thus, the degree to which C_{60} is present in the environment becomes a very important question.

Acknowledgment. This work was supported by NSF Grants CHE89-11916 and CHE 89-21133 (F.N.D. and R.L.W.) and NIH Grant GM-20080.

FEATURE ARTICLE

How To Observe the Elusive Resonances in H or D + H_2 $\rightarrow$ H_2 or HD + H Reactive Scattering

William H. Miller* and John Z. H. Zhang†

Department of Chemistry, University of California, Materials and Chemical Sciences Division, Lawrence Berkeley Laboratory, Berkeley, California 94720 *(Received: August 14, 1990)*

Short-lived collision complexes in H or D + H_2 ($v = j = 0$) $\rightarrow$ H_2 or HD (v', j') + H reactive scattering give rise to broad resonance structure. Though this structure is not observable in the energy dependence of the *integral* cross section, it is readily seen in the energy dependence in the *differential* cross section $\sigma(\theta,E)$, as a peak along a line in the E-θ plane. The equation of this resonance line is $E = E_r(J(\theta))$, where $E_r(J)$ is the resonance energy as a function of total angular momentum J (i.e., the rotational quantum number of the complex) and $J(\theta)$ is the inverse function of $\Theta(J)$, the effective classical deflection function for the transition. Observation of this resonance structure requires cross sections to individual final (v', j') states; it is quenched by summing over j'. It is even more enhanced in cross sections to specific final m' states with $m' \neq 0$. (m' is the helicity of the final state, the projection of the final diatomic molecule rotational angular momentum onto the final relative translational velocity vector.) The results reported are all from rigorous three-dimensional quantum mechanical reactive scattering calculations for these cross sections.

1. Introduction

Resonances continue to attract a great deal of attention in state-to-state reactive scattering and also other areas of chemical dynamics.[1] A scattering resonance is due to a short-lived complex of the two colliding species. Collision complexes exist also in classical mechanics[2] but do not produce resonance behavior because in classical mechanics the energy of the collision complex is not required to be quantized. (In the early days of quantum mechanics the quantization of metastable states was referred to as "weak quantization"[3] because the resonance structure has a finite width Γ in energy space that is related to the finite lifetime of the complex, $\tau = \hbar/\Gamma$. Infinitely long-lived states, i.e., bound states, have $\Gamma = 0$ and thus correspond to "strong quantization".) Quantization of the collision complex, i.e., resonance structure, is thus a purely quantum mechanical phenomenon that can be understood semiclassically[4] as an interference effect between the

† Current address: Department of Chemistry, New York University, New York, NY 10003.

(1) (a) Truhlar, D. G., Ed. *Resonances in Electron-Molecule Scattering, van der Waals Complexes, and Reactive Chemical Dynamics Calculations*; ACS Symposium Series No. 263; American Chemical Society: Washington, D.C., 1984. (b) Schatz, G. C. *Ann. Rev. Phys. Chem.* **1988**, *39*, 317.
(2) Brumer, P.; Karplus, M. *Discuss. Faraday Soc.* **1973**, *55*, 80.
(3) Kemble, E. C. *The Fundamental Principles of Quantum Mechanics with Elementary Applications*; Dover: New YOrk, 1958; pp 178-195.

0022-3654/91/2095-0012$02.50/0

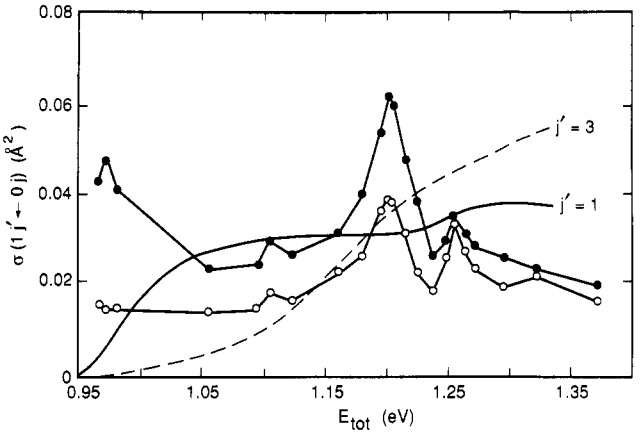

Figure 1. Integral cross section for the para → ortho reaction H + $H_2(v = 0, j) \rightarrow H_2(v' = 1, j')$ + H as a function of total energy. The solid and dashed lines are the theoretical results of ref 10 for $j' = 1$ and 3, respectively; they both are the rotational ground state ($j = 0$). The solid and open circles are the corresponding experimental results of ref 8 for which the initial rotational state is a Boltzmann distribution of para states (52% $j = 0$, 48% $j = 2$).

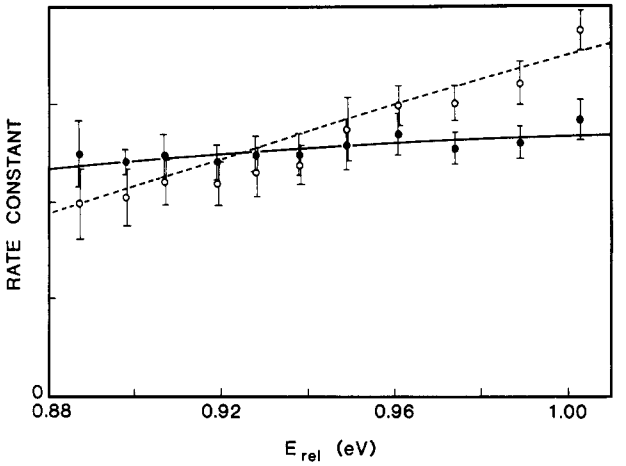

Figure 2. Same as Figure 1, except the points are the experimental results of ref 15. (Precisely speaking, the experiments in both Figures 1 and 2 measure rate constants.) These experimental values have been normalized to the theoretical results (which have been appropriately averaged over the experimental energy resolution), though the $j' = 1$ and 3 values are absolute relative to one another; see ref 15 for more details. Since E_{tot} of Figure 1 is related to E_{rel} here by (for $j = 0$) $E_{tot} \cong E_{rel}$ + 0.27 eV, the energy scale here covers the range $E_{tot} \cong 1.15$–1.28 eV in Figure 1.

different complex-forming classical trajectories that contribute to the reaction; this semiclassical picture is discussed and illustrated more completely in the Appendix. The resonance energies can typically be assigned[5] vibrational and rotational quantum numbers for the collision complex in essentially the same way as for vibrational–rotational eigenvalues of a stable molecule. For a linear A···B···C complex in an A + BC → AB + C atom–diatom reaction, for example, the resonance energies are characterized by symmetric, antisymmetric, and bending (doubly degenerate) vibrational quantum numbers (v_s, v_a, v_b), and the total angular momentum quantum number J for rotation of the linear "molecule". (In nuclear and elementary particle physics these resonance states are often referred to as new "particles", e.g., the H_3 "particle" in the case of on H + H_2 scattering resonance.)

Resonance structure in the fundamental H + H_2 → H_2 + H family of reactions was seen many years[6] ago in quantum scattering calculations for the collinear version of the reaction and then later[7] in the more physically relevant three-dimensional version. Wu and Levine[6b] were the first to explain the mechanism of complex formation in this reaction. The resonance structure is typically seen as a peak (or a minimum) in the reaction probability as a function of energy.

Considerable excitement was thus generated recently by Nieh and Valentini's report[8] showing resonance structure in the energy dependence of the integral (i.e., integrated over scattering angles) cross section for the para → ortho reaction

$$H + H_2 (v = 0, j = 0 \text{ and } 2) \rightarrow H_2 (v' = 1, j' = 1 \text{ and } 3) + H$$

To briefly recap this recent history[9] of resonances in the H + H_2 reaction, Figure 1 shows these experimental cross sections, compared to the results of rigorous three-dimensional quantum reactive scattering calculations by Zhang and Miller.[10] (These calculations included only the $j = 0$ initial rotational state of H_2, but earlier calculations by the Truhlar–Kouri[11] group for low values of total angular momentum J showed that including $j = 2$ had little effect on the results.) Later calculations by Manolopoulos and Wyatt[12] and then by Launay and LeDourneuf[13] upheld the theoretical cross sections, and other calculations[14] also showed that the theoretical results did not change drastically with modest changes in the potential surface. Though there was quite good experimental–theoretical agreement with the *magnitude* of the integral cross sections in Figure 1, the energy dependence of the theoretical cross section showed absolutely no hint of the structure that was attributed to resonance behavior. The situation has apparently been resolved by very recent experimental results from Zare's group[15] (reported[9b] at the Boston meeting of the American Chemical Society, April 22–27, 1990) that show no resonant-like structure in the energy dependence of the integral cross sections in Figure 1. These new experimental results are shown in Figure 2 and are seen to be in truly excellent agreement with the theoretical calculations. (Note that the range of energy in Figure 2 corresponds to the interval $E_{tot} \cong 1.15$–1.28 eV in Figure 1, which shows the prominent structure.)

Does this then mean that the results of short-lived collision complexes in the H + H_2 → H_2 + H (and also D + H_2 → HD + H) reaction are unobservable? Fortunately, the answer is no, and the main purpose of this article is to show how they are manifest. Though the resonances are indeed too broad to be seen in the *integral* cross sections, they do appear quite clearly in the energy dependence of the *differential* cross section (i.e., the angular distribution).[16] They are seen most clearly in a three-dimensional plot of the cross section $\sigma(\theta,E)$ as a function of the two variables θ and E, the center of mass scattering angle, and the total energy; the resonance structure is a peak in $\sigma(\theta,E)$ along the line $E = E_r(J(\theta))$ in the E–θ plane, where $E_r(J)$ is the resonance energy as a function of the total angular momentum J (the rotational

(4) Miller, W. H. *Adv. Chem. Phys.* **1975**, *30*, 99–105.
(5) (a) Colton, M. C.; Schatz, G. C. *Chem. Phys. Lett.* **1986**, *124*, 256. (b) Bowman, J. M. *Chem. Phys. Lett.* **1986**, *124*, 260. (c) Garrett, B. C.; Schwenke, D. W.; Skodje, R. T.; Thirumalai, D.; Thompson, T. C.; Truhlar, D. G. Reference 1a, p 375. (d) Pollak, E.; Wyatt, R. E. *J. Chem. Phys.* **1984**, *81*, 1801. (e) Pollak, E. *Chem. Phys. Lett.* 1987, *137*, 171. (f) Hipes, P. G.; Kuppermann, A. *Chem. Phys. Lett.* **1987**, *133*, 1.
(6) (a) Truhlar, D. G.; Kuppermann, A. *J. Chem. Phys.* **1970**, *52*, 3841. (b) Levine, R. D.; Wu, S.-F. *Chem. Phys. Lett.* **1971**, *11*, 557. (c) For a comprehensive review of the early history of the H + H_2 reaction, see: Truhlar, D. G.; Wyatt, R. E. *Ann. Rev. Phys. Chem.* **1976**, *27*, 1.
(7) Schatz, G. C.; Kuppermann, A. *Phys. Rev. Lett.* **1975**, *35*, 1266.
(8) Nieh, J. C.; Valentini, J. J. *Phys. Rev. Lett.* **1988**, *60*, 519; *J. Chem. Phys.* **1990**, *92*, 1083.
(9) (a) A more complete discussion is given in: Miller, W. H. *Ann. Rev. Phys. Chem.*, in press. (b) Also see: Borman, S. *Chem. Eng. News* **1990**, *68*, 32–37.
(10) Zhang, J. Z. H.; Miller, W. H. *Chem. Phys. Lett.* **1988**, *153*, 465.
(11) Mladenovic, M.; Zhao, M.; Truhlar, D. G.; Schwenke, D. W.; Sun, Y.; Kouri, D. J. *Chem. Phys. Lett.* **1988**, *146*, 358.
(12) Manolopoulos, D. E.; Wyatt, *Chem. Phys. Lett.* **1989**, *159*, 123.
(13) Launay, J. M.; LeDourneuf, M. *Chem. Phys. Lett.* **1989**, *163*, 178.
(14) (a) Manolopoulos, D. E.; Wyatt, R. E. *J. Chem. Phys.* **1990**, *92*, 810. (b) Auerbach, S. M.; Zhang, J. Z. H.; Miller, W. H. *J. Chem. Soc., Faraday Trans.* **1990**, *86*, 1701.
(15) Kliner, D. A. V.; Adelman, D. E.; Zare, R. N. The H + para-H_2 Reaction: Influence of Dynamical Resonances on $H_2(v'=1, j'=1$ and 3) Integral Cross Sections. Preprint.
(16) Continetti, R. E.; Zhang, J. Z. H.; Miller, W. H. *J. Chem. Phys.*, in press.

quantum number of the collinear complex) and $J(\theta)$ is the inverse function of $\Theta(J)$, the effective classical deflection function for the transition. There is one cautionary note, however: observation of resonance features requires cross sections for specific final vibrational-rotational states (v', j') of the product molecule; summing over final rotational states j' destroys the resonance structure. The resonance peak is even more prominent in cross sections to specific final m' states with $m' \neq 0$. (m' is the final helicity quantum number, the projection of the molecule's rotational angular momentum onto the final relative translational velocity vector.)

All results shown below are from Zhang and Miller's three-dimensional quantum reactive scatttering calculations[10,17] and thus should be the essentially exact results for the assumed (LSTH[18]) potential energy surface. They thus serve as predictions of the features that can be observed in reactive collisions with sufficient energy, angular, and quantum state resolution. The cross sections to specific final helicity states are reported here for the first time.

2. Summary of Cross Section Formulas

It is useful first to summarize the basic formulas that express the various cross sections of interest.[19] The most detailed observable for the atom–diatom reaction

$$A + BC(vjm) \rightarrow AB(v'j'm') + C \tag{2.1}$$

is the complete state-selected, state-detected differential cross section, as a function of scattering angle θ and total energy E:

$$\sigma_{v'j'm'\leftarrow vjm}(\theta,E) = |f_{v'j'm'\leftarrow vjm}(\theta,E)|^2 \tag{2.2a}$$

where the scattering amplitude is

$$f_{v'j'm'\leftarrow vjm}(\theta,E) = (2ik_{vj})^{-1} \sum_{J=0} (2J+1) d^J_{m'm}(\theta)\, S^J_{v'j'm',vjm}(E) \tag{2.2b}$$

Here J is the total angular momentum quantum number for the three-atom system, $d^J_{m'm}(\theta)$ is the Wigner rotation function[20] (e.g., $d^J_{00}(\theta) = P_J(\cos\theta)$), v and j denote the vibrational and rotational quantum numbers of the diatomic molecules, and m is the helicity quantum number, the projection of the diatom rotational angular momentum onto the relative (atom–diatom) translational velocity vector before (for m) and after (for m') the collision. (I.e., the space-fixed quantization axis is different for the initial and final rotational states.) The S matrix is obtained by solving the reactive scattering Schrödinger equation with appropriate scattering boundary conditions.[17] The integral cross section is obtained by integrating over the scattering angle:

$$\sigma_{v'j'm'\leftarrow vjm}(E) \equiv 2\pi \int_0^\pi d\theta \sin(\theta) \sigma_{v'j'm'\leftarrow vjm}(\theta,E) = \frac{\pi}{k_{vj}^2} \sum_{J=0} (2J+1) |S^J_{v'j'm',vjm}(E)|^2 \tag{2.2c}$$

The differential cross section of eq 2.2a,b thus involves a *coherent* sum over J(i.e., one sums and then squares), while the integral cross section eq 2.2c is given by an *incoherent* sum (a sum of squares of S matrix elements). It is also useful to define the reaction probability:

$$P_{v'j'm',vjm}(J,E) = |S^J_{v'j'm',vjm}(E)|^2 \tag{2.3}$$

When the helicity quantum number m' is not indicated as a label on a cross section or reaction probability, it has been summed over, e.g.

$$P_{v'j',00}(J,E) \equiv \sum_{m'} P^J_{v'j'm',00}(J,E) \tag{2.4a}$$

$$\sigma_{v'j'\leftarrow 00}(\theta,E) \equiv \sum_{m'} \sigma_{v'j'm'\leftarrow 00}(\theta,E) \tag{2.4b}$$

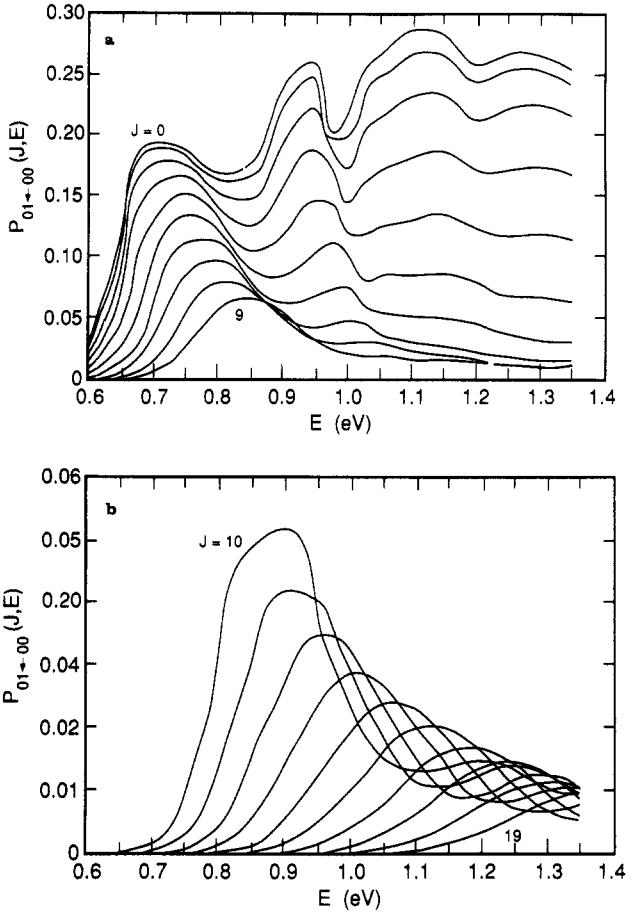

Figure 3. (a) Reaction probabilities (eqs 2.3a, 2.4a) for $H + H_2(v = j = 0) \rightarrow H_2(v' = 0, j' = 1) + H$ as a function of total energy E for various values of total angular momentum J = 0–9. (b) Same for J = 10–19.

All applications in this paper are for the ground initial state of H_2, $v = j = 0$, and thus also $m = 0$.

3. Broad and Narrow Resonances: A Qualitative Discussion

For this discussion we consider a scattering resonance characterized by a single set of vibrational quantum numbers of the collision complex. The resonance energy $E_r(J)$ depends on the total angular momentum quantum number approximately as a linear rigid rotor:

$$E_r(J) \cong E_0 + BJ(J+1) \tag{3.1}$$

and the width $\Gamma(J) \cong \Gamma$ is assumed to be independent of J. The resonance structure in the reaction probability $P(J,E)$ has the generic Lorentzian/Breit–Wigner form[21]

$$P(J,E) \propto \{[E - E_r(J)]^2 + (\Gamma/2)^2\}^{-1} \tag{3.2}$$

Figure 3 shows an example of such reaction probabilities for the reaction

$$H + H_2(v = j = 0) \rightarrow H_2(v' = 0, j' = 1) + H \tag{3.3}$$

where we focus attention on the lowest energy resonance feature for J = 0, 1, ..., 19. (The width Γ actually does depend weakly on J, but it increases by less than a factor of 2 from J = 0 to 19.) Figure 4 shows a plot of $E_r(J)$ (i.e., the position of the peak in the P versus E curves of Figure 3) versus $J(J+1)$ for this resonance, indicating that eq 3.1 is indeed a good approximation for the J dependence of the resonance energy.[22] The "experimental"

(17) Zhang, J. Z. H.; Miller, W. H. (a) *Chem. Phys. Lett.* **1989**, *159*, 130; (b) *J. Chem. Phys.* **1989**, *91*, 1528.
(18) (a) Siegbahn, P.; Liu, B. *J. Chem. Phys.* **1978**, *68*, 2457. (b) Truhlar, D. G.; Horowitz, C. J. *J. Chem. Phys.* **1978**, *68*, 2466; **1979**, *71*, 1514.
(19) See, for example: Miller, W. H. *J. Chem. Phys.* **1969**, *50*, 407.
(20) Rose, M. E. *Elementary Theory of Angular Momentum*; Wiley: New York, 1957; pp 52ff.
(21) See, for example: Miller, W. H. *J. Chem. Phys.* **1970**, *52*, 543.
(22) The centrifugal distortion constant D_e—the coefficient of a $[J(J+1)]^2$ term in eq 3.1—is given for a linear molecule by $D_e = -4B^3/(\hbar\omega_s)^2$; see: Herzberg, G. *Molecular Spectra and Molecular Structure I. Spectra of Diatomic Molecules*; Van Nostrand: Toronto 1950; p 103. Here, ω_s is the symmetric stretch frequency, and with $\hbar\omega_s$ = 2047 cm^{-1} one obtains $D_e = -0.86 \times 10^{-3}$ cm^{-1}. Thus the $D_e[J(J+1)]^2$ term is 2% of the $BJ(J+1)$ term for J = 10 and still only 8% at J = 20.

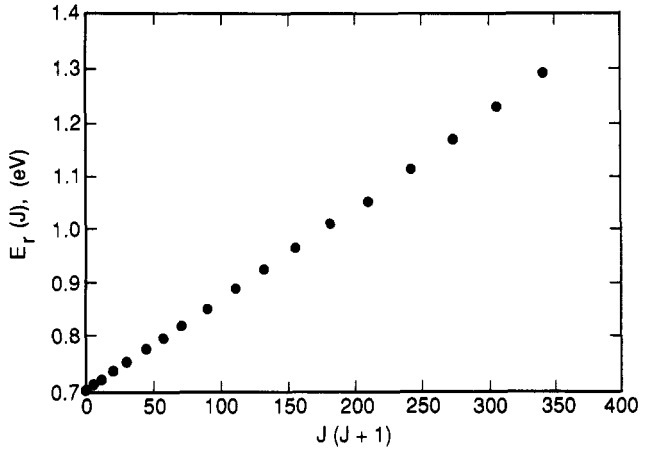

Figure 4. Resonance energy as a function of total angular momentum J, for the same transition as in Figure 3; i.e., $E_r(J)$ is the energy of the local maximum in the $P(J,E)$ versus E curves in Figure 3.

rotation constant B from this plot (i.e., the slope of the approximately straight line) is $\sim$12–13 cm^{-1}, compared to $\sim$10 cm^{-1} for rigid H···H···H at its transition-state geometry.

We will refer to resonances as "broad" or "narrow" depending on the ratio of the width Γ to the *spacing* of resonance energies with respect to the total angular momentum quantum number

$$\Gamma/\Delta E(J) \tag{3.4a}$$

where the spacing $\Delta E(J)$ is given by

$$\Delta E(J) \cong \frac{d}{dJ} E_r(J) \equiv E_r'(J) \tag{3.4b}$$

In light of eq 3.1 one has

$$E_r'(J) = B(2J + 1) \tag{3.4c}$$

Since $E_r'(J)/\hbar$ may also be thought of as the classical frequency for rotation of the linear complex, the ratio in eq 3.4a may also be interpreted as

$$\Gamma/\Delta E(J) = \tau_{rot}/\tau_{life} \tag{3.5}$$

i.e., the ratio of the time for a rotation of the complex to its lifetime ($\tau_{life} \cong \hbar/\Gamma$). A "narrow" resonance ($\Gamma/\Delta E \ll 1$, $\tau_{life} \gg \tau_{rot}$) is thus one that lives long enough to rotate many times, while the converse is true for a "broad" resonance. The resonances in the H + H_2 and D + H_2 reactions under consideration in this paper will be seen to be "broad".

Another perspective of "broad" and "narrow" resonances is revealed by considering the reaction probability eq 3.2 as a function of J for fixed E. The resonance condition

$$E = E_r(J)$$

also defines the resonance angular momentum $J_r(E)$ as a function of E, and if one expands eq 3.2 for J near $J_r(E)$, then

$$P(J,E) \propto \{[E_r'(J)(J - J_r)]^2 + (\Gamma/2)^2\}^{-1} \tag{3.6a}$$

$$\propto \left[(J - J_r)^2 + \left(\frac{\Delta J}{2}\right)^2\right]^{-1} \tag{3.6b}$$

where

$$\Delta J = \Gamma/E_r'(J) \tag{3.6c}$$

As a function of J, therefore, P also has a Lorentzian form, and its width ΔJ in eq 3.6c is seen to be the width-to-spacing ratio eq 3.4, which defines "broad" and "narrow" resonances. Since the integral cross section is a sum of $P(J,E)$ over J (cf. eq 2.2c)

$$\sigma(E) \propto \sum_J (2J + 1)P(J,E) \tag{3.7}$$

another meaning of ΔJ is clear; it is approximately the number of J values that contribute to the partial wave sum for the resonance contribution to the integral cross section $\sigma(E)$ for a given value of E. $\Delta J \ll 1$ (a narrow resonance) thus means that only one value of J will make a contribution to the resonance structure for a given E, so that resonance structure would be observed in the energy dependence of the integral cross section $\sigma(E)$. $\Delta J \gg 1$, however, means that many ($\sim\Delta J$) values of J contribute to $\sigma(E)$, so that resonance structure will be quenched by the overlapping resonances (inhomogeneous broadening).

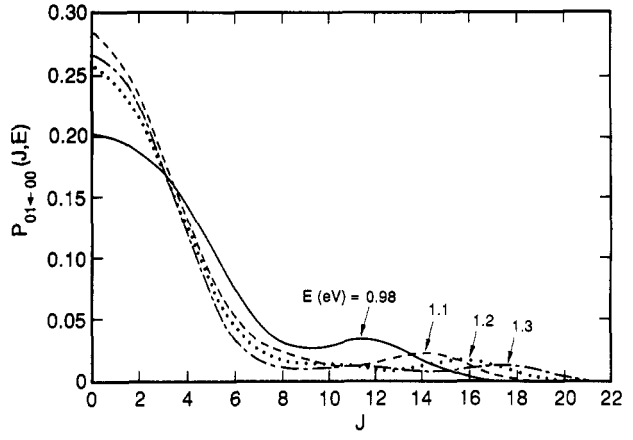

Figure 5. Reaction probabilities, for the same transition as in Figure 3, as a function of J for several values of E. The arrows indicate the resonances positions for the various values E.

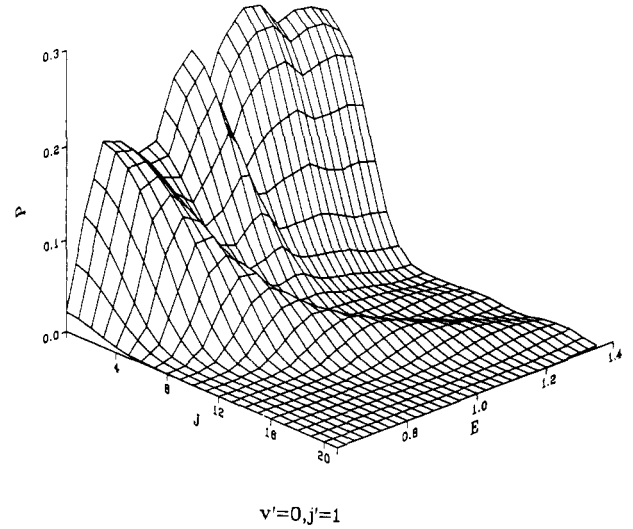

Figure 6. Three-dimensional plot of the reaction probability $P(J,E)$ as a function of J and E, for the same transition as in Figure 3.

Figure 5 shows a plot of $P(J,E)$ versus J for several values of E for reaction eq 3.3. The resonance feature is clearly discernible, and one can estimate the value $\Delta J \cong$ 3–4 for these energies. This is thus a "broad" resonance in the present sense.

Finally, Figure 6 shows the reaction probability $P(J,E)$ for reaction 3.3 in a three-dimensional plot, which allows one to see the J and E dependence simultaneously. The Lorentzian peak now appears as a "ridge" along the resonance line $E = E_r(J)$.

4. Broad and Narrow Resonances: The Differential Cross Section/Angular Distribution

As noted in the previous section, "narrow" resonances show interesting resonance structure in the energy dependence of the integral cross section because the resonance takes place in only one partial wave (one value of J) over the relevant energy region. In this case the differential cross section typically is *un*interesting. Thus if $J_r(E)$ is the value of J undergoing the resonance behavior in a given range of E, the resonance contribution to the differential cross section is

$$\sigma(\theta,E) \propto |d^{J_r}_{m',m}(\theta)|^2 \tag{4.1a}$$

and if m, $m' \ll J$, this is approximately

$$\sigma(\theta,E) \propto 1/\sin\theta \tag{4.1b}$$

This forward–backward peaking in the angular distribution is a well-known[23] result when the collision complex lives for many rotational periods. Narrow resonances thus show interesting features in the energy dependence of the integral cross section, but the angular distribution is rather uninteresting; i.e., forward–backward symmetry of the angular distribution tells one only that the complex lives long enough to rotate many times, $\tau_{rot}/\tau_{life} = \Gamma/\Delta E \ll 1$, i.e., that the resonance is "narrow".

Broad resonances show resonance structure in $P(J,E)$ (cf. Figure 6), but none of this survives in the *integral* cross section because the sum over J has contributions from a number ($\sim\Delta J$) of values of J. Because of this, however, the **S** matrix element in the partial wave sum for the scattering amplitude (eq 2.2b) is a sufficiently smooth function of J that the Ford and Wheeler[24] semiclassical stationary phase approximation can thus be used to evaluate the sum over J. Miller[25] has shown explicitly how this is generalized for the present case of atom–diatom reactive collisions. In eq 2.2b one replaces the sum over J by an integral over J, uses the WKB approximation for the Wigner function,[26] writes the **S** matrix as

$$\mathbf{S}^J = |\mathbf{S}(J)|e^{i\phi(J)} \tag{4.2}$$

and evaluates the integral over J via the stationary phase approximation (assuming that the magnitude of the **S** matrix is a smooth function of J). The principal difference from the Ford and Wheeler case of elastic scattering is the appearance of the Wigner function $d^J_{m'm}(\theta)$ rather than the Legendre polynomial $P_J(\cos\theta)$, but the WKB approximation for the former is a simple generalization of that for the latter.

The result of this semiclassical calculation is[25]

$$\sigma(\theta,E) = \sigma_{el}(\theta,E)\ P(J(\theta),E) \tag{4.3}$$

where $\sigma_{el}(\theta,E)$ is an elastic-like differential cross section

$$\sigma_{el}(\theta,E) = (J + \tfrac{1}{2})[k^2 \sin\theta|\Theta'(J)|(1 - m^2/J^2)^{1/2}(1 - m'^2/J^2)^{1/2}]^{-1} \tag{4.4}$$

with $J = J(\theta)$ determined by the stationary phase condition

$$\Theta(J) = \theta \tag{4.5}$$

where the classical deflection function $\Theta(J)$ is given in terms of the J derivative of the phase of the **S** matrix by

$$\Theta(J) = \cos^{-1}\left[\frac{mm'}{J^2} + (1 - m^2/J^2)^{1/2}(1 - m'^2/J^2)^{1/2}\cos\phi'(J)\right] \tag{4.6}$$

(For $m = m'$ 0, eqs 4.4–4.6 revert to the standard Ford and Wheeler result.) The probability function in eq 4.3 is the reaction probability

$$P(J,E) = |S^J(E)|^2 \tag{4.7}$$

evaluated at the value $J(\theta)$ determined by the stationary phase relation, eq 4.5.

Assuming that $\sigma_{el}(\theta,E)$ is a smooth function, structure in $P(J,E)$ as a function of J and E is thus transferred to structure in $\sigma(\theta,E)$ as a function of θ and E, through the $\theta(J)/J(\theta)$ functionality brought about by the stationary-phase approximation for summing/integrating over J. This is the sense in which the stationary-phase approximation unfolds the partial wave sum, at least approximately.[27]

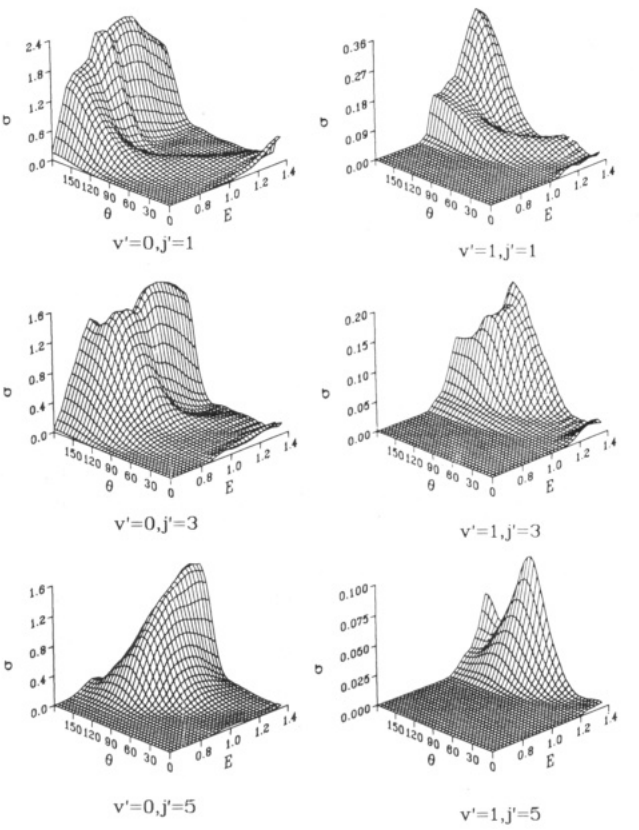

Figure 7. Three-dimensional plot of the differential cross section $\sigma(\theta,E)$ as a function of θ and E, for the transitions $H + H_2(v = j = 0) \rightarrow H_2(v', j') + H$, for various final states (v', j').

One thus has a kind of complementarity: *narrow* resonances show interesting structure in the energy dependence of the *integral* cross section, but further information given by the differential cross section is rather trivial. *Broad* resonances, on the other hand, show interesting resonance structure in the θ–E dependence of the *differential* cross section, while such structure is quenched in the integral cross section.

Figure 7 shows a three-dimensional plot of $\sigma(\theta,E)$ as a function of θ and E, for the $H + H_2(v = j = 0) \rightarrow H_2(v', j') + H$ reaction for several find vibrational–rotational states (v', j'). For $v' = 0$ and $j' = 1$, 3, the peak along the resonance line $E = E_r(J(\theta)$ is clearly discernible, as it also is for final state $v' = j' = 1$ (this a resonance with a different set of vibrational quantum numbers). Higher values of j' in all cases, though, tend to obscure the resonance structure.

Finally, we note that the semiclassical stationary-phase analysis that leads to eq 4.3 and thus maps resonance structure in $P(J,E)$ into that for $\sigma(\theta,E)$ has also been used by Wyatt et al.[28] and Hayes and Walker[29] to discuss resonances in the $F + H_2 \rightarrow HF + H$ reaction. The present work, however, is the first time that such structure in $\sigma(\theta,E)$ has been explicitly demonstrated. It should be noted also that eq 4.3 is a well-known qualitative relation that results from a number of different approximate treatments of

(23) Miller, W. B.; Safron, S. A.; Herschbach, D. R. *Discuss. Faraday Soc.* **1967**, *44*, 108.
(24) Ford, K. W.; Wheeler, J. A. *Ann. Phys. (N.Y.)* **1959**, *7*, 259.
(25) Miller, W. H. *J. Chem. Phys.* **1970**, *53*, 1949.
(26) Brussard, P. J.; Tolhoek, H. A. *Physica* **1957**, *23*, 955.

(27) As an aside, we note that if the scattering amplitude itself, eq 2.2b, were observable, then one could easily and exactly transform from θ space to J space, by exploiting the orthogonality of the Wigner functions,[20] and thus obtain the **S** matrix (and therefore reaction probabilities) as a function of J and E:

$$S^J_{v'j'm',vjm}(E) = ik_{vj}\int_0^\pi d\theta \sin(\theta) d^J_{m'm}(\theta)^* f_{v'j'm'\leftarrow vjm}(\theta,E)$$

Unfortunately, though, one cannot easily obtain the scattering amplitude from the cross section (the "phase problem").

(28) (a) Redmon, M. J.; Wyatt, R. E. *Chem. Phys. Lett.* **1979**, *63*, 209. (b) Wyatt, R. E.; McNutt, J. F.; Redmon, M. J. *Ber. Bunsen-Ges Phys. Chem.* **1982**, *86*, 437.
(29) Hayes, E. F.; Walker, R. B. (a) Reference 1, p 493; (b) *J. Phys. Chem.* **1984**, *88*, 3318.

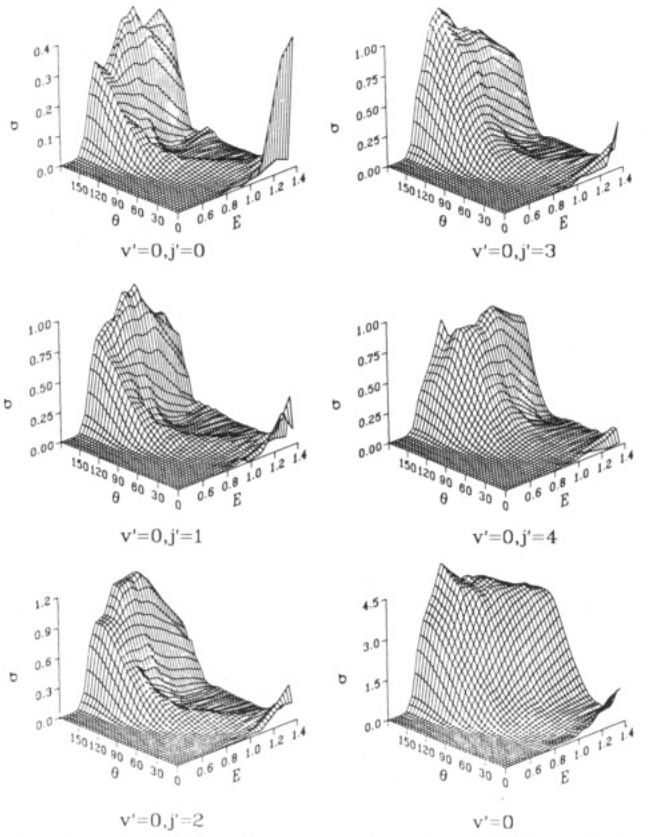

Figure 8. Same as Figure 7, except for the reaction D + $H_2(v = j = 0)$ → HD($v' = 0, j'$), for various final rotational states j'. The figure labeled $v' = 0$ is the cross section summed over all values of j'.

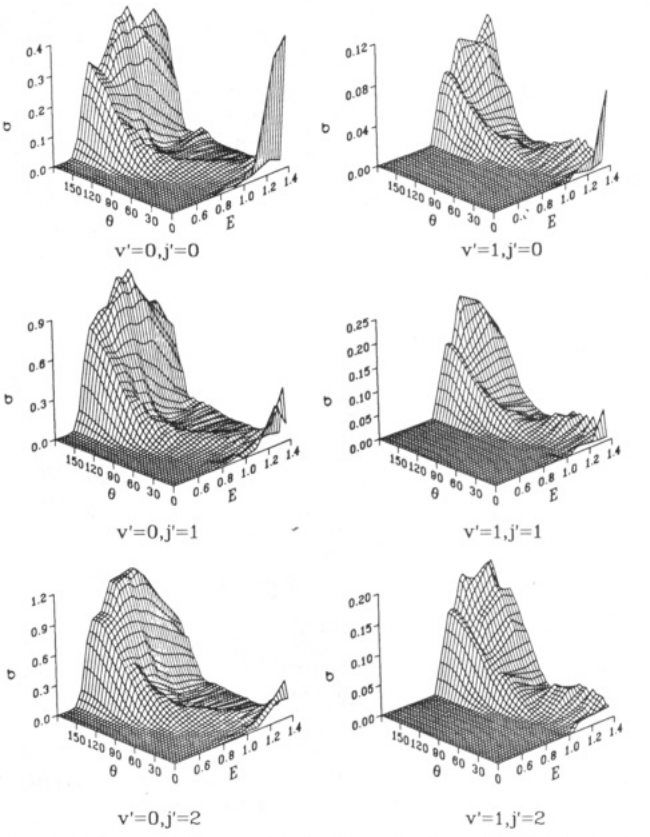

Figure 9. Same as Figure 8, D + $H_2(v = j = 0)$ → HD(v', j') + H, except for $v' = 0$ and 1, for various values of j'. (The principle resonances seen in the $v' = 0$ and $v' = 1$ cross sections correspond to different resonance vibrational quantum numbers.)

reactive scattering, e.g., the optical model[30] and the distorted wave Born approximation.[31]

5. More Results

Here we present some additional energy-dependent differential cross sections that show the type of resonance behavior discussed above. Figure 8 shows $\sigma(\theta,E)$ for the D + H_2 reaction[16,17b]

$$D + H_2(v = j = 0) \rightarrow HD(v', j') + H \qquad (5.1)$$

for $v' = 0$ and $j' = 0$–4 (and also summed over j'). A resonance peak along the line $E = E_r(J(\theta))$ shows up quite clearly for $j' = 0$–2 and somewhat more weakly for $j' = 3, 4$. Significantly, the cross section summed over j' shows no discernible resonance-like feature. Figure 9 compares the cross sections for $v' = 0$ with those for $v' = 1$, for $j' = 0$–2. The principal resonances seen for $v' = 0$ and $v' = 1$ correspond to different resonance vibrational quantum numbers, but the resonance structure for $v' = 1$ appears to be no less distinct than that for $v' = 0$.

Finally, we note that the state-to-state cross sections shown so far are not the most detailed ones possible, for they have been summed over the final helicity quantum number m'. It is thus of interest to see if the resonance features are revealed any more clearly in the cross sections to specific final m' states. We surmise that this might be true because is is known that these collinearly dominant reactions tend to conserve helicity.[32] Since the initial state has $m = 0$, the cross section for $m' = 0$ is thus expected to be the largest. Therefore most of the "direct" scattering, which tends to mask the resonant contribution, might be expected to be in the $m' = 0$ channel. In addition, the fact that the resonance lives long enough to rotate (at least more than the "direct" scattering contribution) means that it may have more Coriolis coupling that will lead to Δm transitions. Both of these arguments suggest that the resonance structure may be more prominent in final states with $m' \neq 0$.

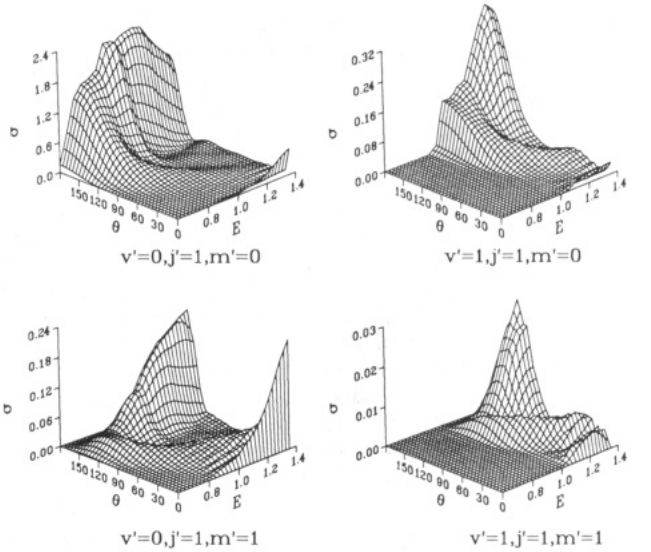

Figure 10. Three-dimensional plot of the completely state resolved differential cross section for H + $H_2(v = j = 0)$ → $H_2(v', j' m')$ + H, as a function of θ and E. Note the σ scale for the $m' = 1$ is an order of magnitude smaller than that for $m' = 0$ final states.

Figure 10 shows such results for the H + H_2 reaction for $j' = 1$, so that $m' = 0$ or 1 (−1 is the same), for $v' = 0$ and 1. (Note that the scale for the $m' = 1$ cross sections is about an order of magnitude smaller than that for the $m' = 0$ cross sections.)

(30) Beck, D.; Greene, E. F.; Ross, J. *J. Chem. Phys.* **1962**, *37*, 2895.
(31) Miller, W. H. *J. Chem. Phys.* **1968**, *49*, 2373.
(32) For example: (a) Elkowitz, A. B.; Wyatt, R. E. *Mol. Phys.* **1976**, *31*, 189. (b) Kuppermann, A.; Schatz, G. C.; Dwyer, J. *Chem. Phys. Lett.* **1977**, *45*, 71. (c) Schatz, G. C. *Chem. Phys. Lett.* **1983**, *94*, 183. (d) Schatz, G. C. In *The Theory of Chemical Reaction Dynamics*; Clary, D. C., Ed.; D. Reidel: Dordrecht, Holland, 1986; p 1.

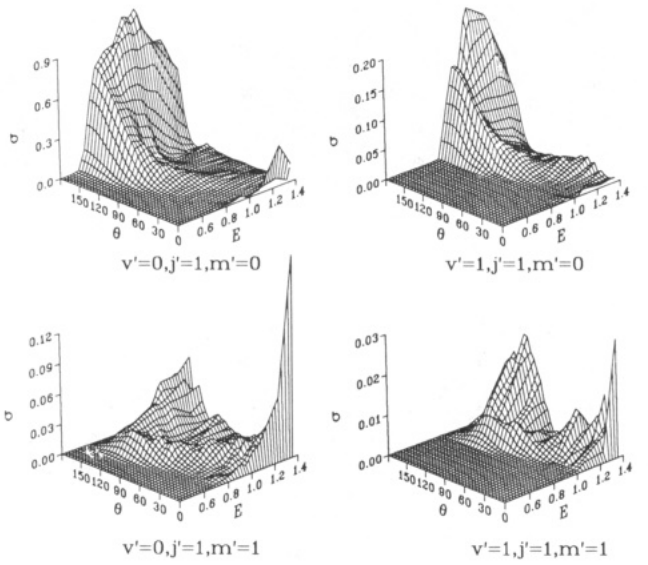

Figure 11. Same as Figure 10, except for the reaction D + $H_2(v = j = 0) \rightarrow HD(v', j', m')$ + H.

Though it is not a dramatic effect, the resonance feature does appear to be more distinct for the $m' = 1$ cross sections than for $m' = 0$ (especially for $v' = 0$).

Figure 11 shows similar results for the D + H_2 reaction, and the conclusion is similar (although the smallest cross section $v' = j' = m' = 1$ has considerable numerical noise).

6. Concluding Remarks

The most important conclusion from the theoretical cross sections presented here is that resonant structure due to short-lived collision complexes in H/D + $H_2 \rightarrow H_2$/HD + H reactive scattering is indeed observable, as a resonance peak in the energy-dependent differential cross section $\sigma(\theta,E)$ along a line in the E–θ plane. The equation for this resonance line is $E = E_r(J(\theta))$, where $E_r(J)$ is the resonance energy as a function of total angular momentum J (i.e., the rotational quantum number of the collision complex), and $J(\theta)$ is the inverse function of $\Theta(J)$, the effective classical deflection function for the specific transition.

Observation of the resonance structure requires that one determine the energy-dependent differential cross sections to specific final vibrational–rotational (v', j') states of the product diatomic molecule (or even better, also to specific final helicity states (v', j', m')). Determining differential cross sections requires a crossed molecular beam experiment, but so far these experiments[33,34] have detected final states by time-of-flight analysis of the final translational energy distribution and have not been able to resolve specific final rotational states j'; the best that has been done is to resolve final vibrational states v', with some convoluted information about the final rotational-state distribution.

To accomplish complete quantum-state resolution of the differential cross section requires that one use a spectroscopic-type product analysis[35]—e.g., laser-induced fluorescence, multiphoton ionization, infrared or Raman spectroscopy, etc.—at each scattering angle in a crossed beam experiment. These experiments have not yet been carried out, but one anticipates that they will be within the next few years. The present theoretical results predict that the effort required to do so will be amply rewarded. A bonus with most spectroscopic detection schemes is that one would likely obtain information about specific final m' states from polarization measurements.

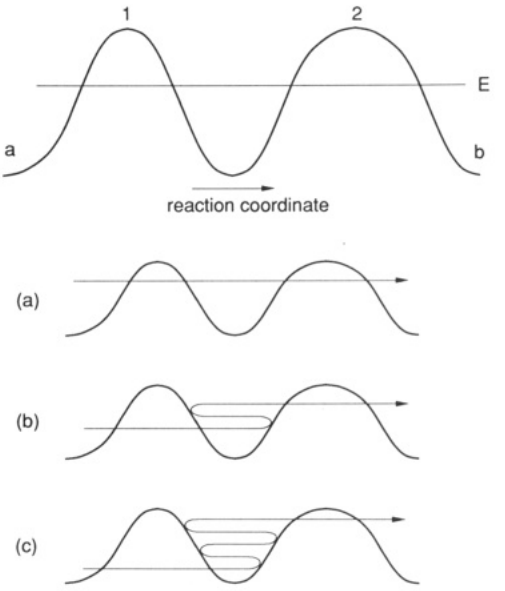

Figure 12. Potential energy versus reaction coordinate for a one-dimensional model of an a → b reaction at energy E. 1 and 2 denote two potential barriers. Parts a–c depict various trajectories that contribute to the a → b reaction: (a) the "straight through" direct trajectory: (b and c) those that make one and two extra oscillations, respectively, in the well between the barriers.

Acknowledgment. We wish especially to thank Drs. Kliner, Adelman, and Zare for sending us their preprint[15] prior to publication and for permission to show some of their new experimental results (Figure 2). This work has been supported by the Director, Office of Energy Research, Office of Basic Energy Sciences, Chemical Sciences Division of the U.S. Department of Energy under Contract No. DE-AC03-76SF00098 and also in part by the National Science Foundation Grant CHE-8920690.

Appendix: Resonances as Interference

It is illuminating to demonstrate explicitly the comment made in the Introduction that quantum mechanical resonance structure arises semiclassically as an interference effect. Figure 12 shows the one-dimensional model in the indicated potential at energy E. (In a multidimensional system the two potential barriers might be "dynamical bottlenecks"[36] rather than actual potential energy barriers.)

The net amplitude for the a → b transition is given semiclassically[37] as a sum of amplitudes for all the different trajectories that contribute (cf. Figure 12a–c):

$$S_{b,a} = e^{i\eta_b}P_2^{1/2}e^{i\phi}P_1^{1/2}e^{i\eta_a} + e^{i\eta_b}P_2^{1/2}e^{i\phi}e^{-i\pi/2}(1-P_1)^{1/2}e^{i\phi}e^{-i\pi/2}(1-P_2)^{1/2}e^{i\phi}P_1^{1/2}e^{i\eta_a} + e^{i\eta_b}P_2^{1/2}e^{i5\phi}[e^{-i\pi/2}(1-P_1)^{1/2}e^{-i\pi/2}(1-P_2)^{1/2}]^2P_1^{1/2}e^{i\eta_a} + \ldots \quad (A.1)$$

Here η_a and η_b are the phases accumulated in the regions before barrier 1 and after barrier 2 (cf. Fig. 12), respectively, ϕ is the phase integral across the well between the barriers

$$\phi \equiv \phi(E) = \int_{well} dx\, (2m[E - V(x)]/\hbar^2)^{1/2}$$

and P_1 and P_2 are the probabilities of tunneling through barriers 1 and 2. The first term in eq A.1 corresponds to the "straight through" trajectory (Figure 12a): reading from right to left, the separate factors in this term arise from motion up to barrier 1 ($e^{i\eta_a}$), tunneling through barrier 1 ($P_1^{1/2}$), motion across the well

(33) Buntin, S. A.; Giese, C.; Gentry, W. R. (a) *J. Chem. Phys.* **1987**, *87*, 1443; (b) *Chem. Phys. Lett.*, in press.

(34) Continetti, R. E.; Balko, B. A.; Lee, Y. T. *J. Chem. Phys.*, in press.

(35) For example: (a) Reference 8, with references to earlier work using coherent anti-Stokes Raman scattering (CARS) spectroscopy. (b) Kliner, D. A. V.; Zare, R. N. *J. Chem. Phys.* **1990**, *92*, 2107 (with references to earlier work using resonance-enhanced multiphoton ionization (REMPI)).

(36) Miller, W. H. *J. Chem. Phys.* **1976**, *65*, 2216.

(37) For example: (a) Berry, M. V.; Mount, K. E. *Rep. Prog. Phys.* **1972**, *35*, 315. (b) Miller, W. H. *Adv. Chem. Phys.* **1974**, *25*, 69.

($e^{i\phi}$), tunneling through barrier 2 ($P_2^{1/2}$), and motion beyond barrier 2 ($e^{i\eta_b}$). The second term in eq A.1 corresponds to the trajectory that makes one extra oscillation in the well (Figure 12b); the various factors in this term are for motion up to barrier 1 ($e^{i\eta_a}$), tunneling through barrier 1 ($P_1^{1/2}$), motion across the well ($e^{i\phi}$), reflection[38] from barrier 2 ($e^{-i\pi/2}(1 - P_2)^{1/2}$), motion back across the well ($e^{i\phi}$), reflection from barrier 1 ($e^{-i\pi/2}(1 - P_1)^{1/2}$), motion back across the well ($e^{i\phi}$), tunneling through barrier 2 ($P_2^{1/2}$), and motion beyond barrier 2 ($e^{i\eta_b}$). The third term in eq A.1 corresponds to the trajectory that makes two extra oscillations in the well (Figure 12c), and the sum of all such terms is thus seen to be a simple geometric series:

$$S_{b,a} = e^{i\eta_b} P_2^{1/2} e^{i\phi} \sum_{k=0}^{\infty} [e^{2i\phi} e^{-i\pi}(1 - P_1)^{1/2}(1 - P_2)^{1/2}]^k P_1^{1/2} e^{i\eta_a} \tag{A.2}$$

which can be easily summed, so that the net reaction probability is finally given by

$$P_{b\leftarrow a} \equiv |S_{b,a}|^2 = \frac{P_1 P_2}{|1 + e^{2i\phi}(1 - P_1)^{1/2}(1 - P_2)^{1/2}|^2} \tag{A.3}$$

For energies well below the tops of the barriers, so that P_1 and $P_2 \ll 1$, eq A.3 takes the simpler form

$$P_{b\leftarrow a} \cong \frac{P_1 P_2}{((P_1 + P_2)/2)^2 + 4\cos^2\phi} \tag{A.4}$$

which is the basis for our further discussion. (For energies high above the barrier, for which P_1 and $P_2 \to 1$, eq A.3 gives $P_{b\leftarrow a} \to 1$, as expected.)

As a function of energy, it is easy to see that the reaction probability $P_{b\leftarrow a}(E)$ of eq A.4 peaks at values of E for which

$$\cos\phi = 0$$

i.e.

$$\phi(E) = (n + 1/2)\pi \tag{A.5}$$

for $n = 0, 1, 2, \ldots$. (The peak value is $4P_1P_2/(P_1 + P_2)^2$, e.g., = 1 for the symmetric case $P_1 = P_2$.) Equation A.5 is the usual semiclassical quantization condition for bounded motion in a potential well. The energies $\{E_n\}$ determined by eq A.5, i.e., the semiclassical eigenvalues for motion in the potential well, are thus the resonances energies, the energies at which $P(E)$ peaks. The fact that this is a result of constructive interference is reinforced by considering eq A.2: at energies for which eq A.5 is true

$$e^{2i\phi} e^{-i\pi} = e^{i(2n+1-1)\pi} = 1$$

and since $(1 - P_1)^{1/2}(1 - P_2)^{1/2} \cong 1$, the sum over k in eq A.2 is (approximately) a sume of 1's and thus very large. Values of E for which eq A.5 is not true lead to destructive interference in the sum of amplitudes and a small net reaction probability, e.g., for $\cos^2\phi = 1$ in eq A.4, $P_{b\leftarrow a} \cong P_1P_2 \ll 1$.

It is not hard to determine the width of these resonance peaks in $P_{b\leftarrow a}(E)$ about a given resonance energy E_n. With a Taylor's series expansion for E near E_n

$$\phi(E) \cong \phi(E_n) + \phi'(E_n)(E - E_n) + \ldots$$

one has

$$\cos^2\phi(E) \cong \cos^2[(n + 1/2)\pi + \phi'(E_n)(E - E_n)]$$
$$\cong \phi'(E_n)^2(E - E_n)^2$$

so that eq A.4 takes on the standard Breit–Wigner/Lorentzian form

$$P_{b\leftarrow a}(E) \propto [(\Gamma/2)^2 + (E - E_n^2)]^{-1}$$

with

$$\Gamma = (P_1 + P_2)/2\phi'(E_n) \tag{A.6}$$

Since one can show from eq A.5 that

$$1/2\phi'(E_n) = (2\pi)^{-1}\,\partial E_n/\partial n$$

eq A.6 has the very intuitive form

$$\Gamma/\hbar = \frac{\omega}{2\pi}(P_1 + P_2) \tag{A.7}$$

where $\omega \equiv \partial E_n/\partial n/\hbar$ is the classical frequency for motion in the well. $\Gamma/\hbar$, the decay rate of the resonance, i.e., collision complex, is thus seen to be the decay rate through barrier 1, $(\omega/2\pi)P_1$, plus that through barrier 2, $(\omega/2\pi)P_2$.

(38) Reflection at a classical turning point induces a phase shift of $-\pi/2$ to go along with the square root of the reflection probability.